Peer-reviewed version available at *Fluids* **2018**, *3*, 54; doi:10.3390/fluids3030054

Article

Encapsulation of Droplets Using Cusp Formation Behind a Drop Rising in a Non-Newtonian Fluid

Raphael Poryles [1]* and Roberto Zenit [1]*

[1] Instituto de Investigaciones en Materiales, Universidad Nacional Autónoma de México, Mexico, DF, 04510
* Correspondence: raphael.poryles_at_yahoo.fr or zenit_at_unam.mx

Abstract: The rising of an oil drop in a non-Newtonian viscous solution is studied experimentally. In this case, the shape of the ascending drop is strongly affected by the non-Newtonian properties of the surrounding liquid. We found that the so-called velocity discontinuity phenomena is observed for drops larger than a certain critical size. Beyond the critical velocity, the formation of a long tail is observed, from which small droplets are continuously emitted. We determined that the fragmentation of the tail results mainly from the effect of capillary effects. We explore the idea of using this configuration as a new encapsulation technique, where the size and frequency of droplets can be well predicted.

Keywords: Drop; Cusp instability; Encapsulation

1. Introduction

The problem of encapsulating droplets of fluid has important implications in the fields of bioengineering and medical research, for instance to encapsulate cells [1]. With the development of microfluidics and lab-on-chip technology to perform analysis on different fluids, the dynamics and size of such droplets has to be well controlled [2–4]. Several techniques have been used to perform such encapsulation, for instance using a T-junctions device [5,6]. To be able to perform such encapsulation at a larger scale in a controlled matter is still to be achieved.

Here we study a new alternative technique to encapsulate oil drops by using the non-Newtonian properties of the surrounding liquid. In the case of an object rising or falling in a non-Newtonian fluid, new and unexpected phenomena appear in comparison with the Newtonian case. The flow surrounding the object can be highly modified, due to the viscoelastic properties of the fluids [7–13]. In the case of a bubble or a drop, a jump discontinuity in its ascending velocity has been observed at a given volume [14–18], as well as a negative wake forming at the rear, creating a modification of the bubble shape, with the appearance of a cusped shape [14,19–21]. These features are the result of the normal stress at the interface of the bubble/drop and the surrounding liquid.

In the case of a drop, a recent study has shown that the cusp of the drop can undergo an instability over a critical volume, where a formation of a long tail appears [19]. They reported that in the case where the drop is Newtonian, a small tail grows, while in the case were the drop is constituted of a viscoelastic fluid, this growth is much larger, over few time the size of the drop. Once the tail is big enough, a second instability occurs, resulting in the tail fragmenting into smaller droplets.

However, a precise study of the dynamics of the breakup of the tail, in the case of a Newtonian drop, has yet to be performed. In this article we present results on the formation of droplets behind an oil drop (Newtonian) rising in a water-polyacrylamide solution (non-Newtonian). First we present the experimental set-up and a characterization of the fluids we used. Then we present the experimental observations, and the different regimes of breakup that were observed. Finally we discuss different aspects of the droplets formations, by relating the velocity and volume of the main drop, the size of the tail appearing behind the drop and the size and frequency of formation of the droplets.

Peer-reviewed version available at Fluids 2018, 3, 54; doi:10.3390/fluids3030054

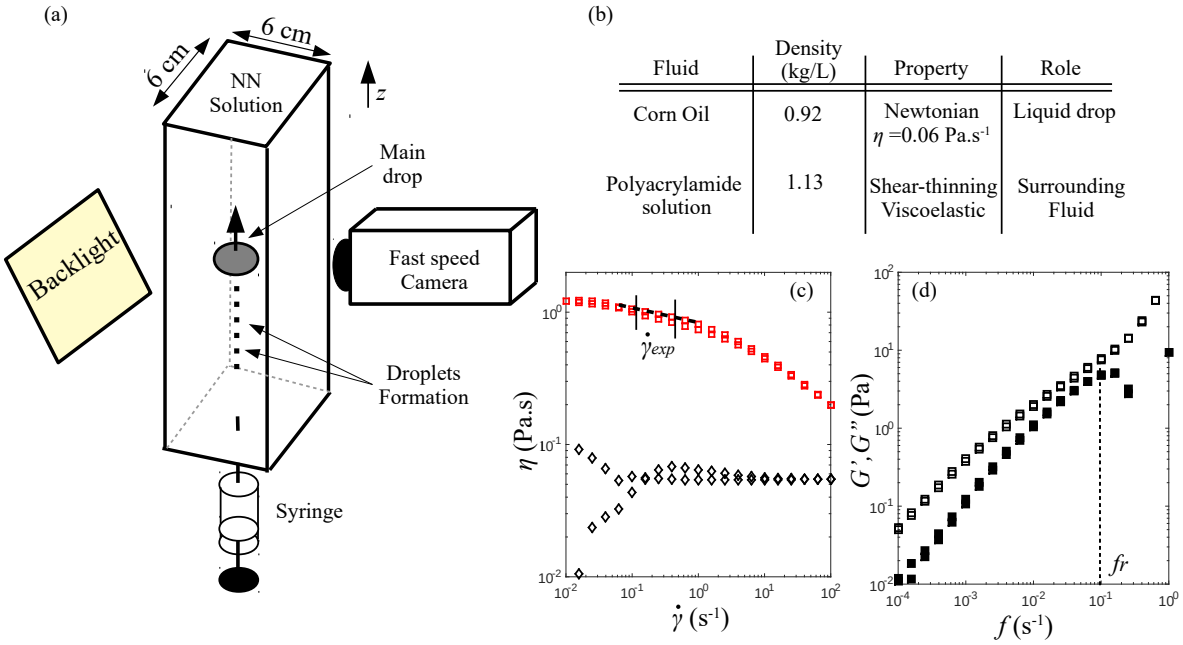

Figure 1. (**a**) Scheme of the experimental set-up. In a vertical glass column with a square base of 6 cm side width and a height of 60 cm, we place a non-Newtonian fluid. An oil drop is injected at the bottom of the column using a plastic syringe. The images are recorded using a fast speed camera (200 fps), and the set-up is backlit using a LED panel. Behind the drop, we observe formation of droplets. (**b**) Table compiling the properties of the two fluids used. Since the oil drop has a lower density and a Newtonian behaviour, it will rise in the surrounding fluid consisting in a water-polyacrylamide solution, which is denser and has shear-thinning and viscoelastic properties.(**c**) Flow curve (measured viscosity η as a function of the shear-rate $\dot{\gamma}$) for the two fluids used. The diamonds represent the oil drop (Newtonian), the squares the polyacrylamide solution (Shear-thinning). $\dot{\gamma}_{exp}$ is the shear-rate observed in our experiment and the dashed line corresponds to the power-law fit. (**d**) Elastic modulus G' (full squares) and viscous modulus G'' (empty squares) as a function of the oscillation frequency for the polyacrylamide solution. A viscoelastic behaviour appears. The relaxation time, τ_r, is estimated from the frequency at which the two modulus are the closest.

2. Experimental set-up and test fluids

The experimental setup consists in a vertical glass column of a height 60 cm (Figure 1**a**). This column is square based with a side width of 6 cm. The setup is filled with a non-Newtonian water-polyacrylamide solution. Alimentary corn oil is injected at the bottom of the column using a plastic syringe with a volume capacity of 5 mL. The set-up is backlit with a LED panel. A fast speed camera (SpeedSence, Phantom) films the rising at a frequency of 200 frames per seconds with a resolution 1632×1200 during 10 seconds. The camera is placed at mid height of the column and films a zone of about 12 cm high. At this point the drop moves at its terminal speed. The scale ratio of the images is of 110 pixels per centimeter, and we measure the diameter, height and position of the drop with a precision of about 2 pixels, so the error is estimated to be smaller than 5 percent for the drop velocity and volume (see section 3).

The properties of the two fluids used are presented in Figure 1**b**. The drop consist in an alimentary corn oil, characterized as Newtonian. For the surrounding fluid, we used a solution composed of a 50% weight solution of water and glycerol (1 kilogram each) in which we added 10 grams of industrial polyacrylamide (Paam, Separan) which are long chains of polymer. The density was measured using a flask with a precise volume of 25 mL which was filled with the different fluids and weighed.

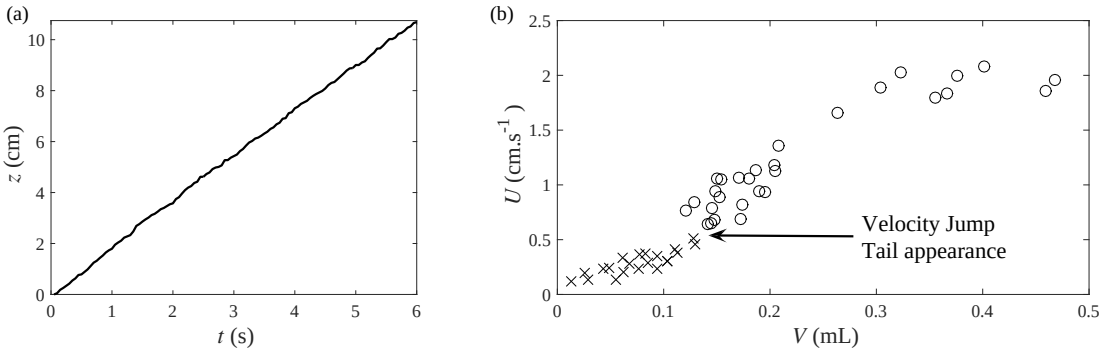

Figure 2. (**a**) Position of the front of the drop as a function of time. This example corresponds to Figure 3**e**. We observe that the rising velocity U stays constant over the 12 cm experiment height. (**b**) Rising velocity U of the drops, as a function of the volume V. We observe a small velocity jump at the moment of the tail appearance for a critical volume V_c = 0.13mL and a critical velocity U_c=0.46 cm.s^{-1}.

Both fluids were characterized using a rheometer (HR, TA Instruments), and we performed two types of tests. We used a plane-plane geometry with a gap of 1 mm, at a fixed temperature of 25 C° and we performed a "flow curve" test, varying the shear rate and measuring the viscosity. The shear rate $\dot{\gamma}$ is varied from 0.01 to 100 s^{-1} with 5 points per decade, with an averaging time of 30 s for each point, and with back and forth variation for reproducibility (going from low shear rate to high, and then reverse). The results are presented in Figure 1**c**. We observe that the corn oil is Newtonian, with a viscosity $\eta_{oil} \approx 0.06$ Pa.s. Important fluctuations are present at low shear rates $\dot{\gamma}$, coming from the precision of the apparatus which is inaccurate for low shear rates at low viscosity. The non-Newtonian fluids, presents clearly a shear-thinning behavior, as the viscosity η_{Paam} (red squares) decreases with the shear rate $\dot{\gamma}$. In our case, we will see later that the shear-rate we will use varies between $\dot{\gamma} = 0.22$ s^{-1} and $\dot{\gamma} = 0.42$ s^{-1}. In this zone, the viscosity follows a power law : $\eta = K\dot{\gamma}^{n-1}$, where $n = 0.87$ and $K = 1.10$ as represented in Figure 1**c**. This exponent n being close to 1 (Newtonian behaviour for $n = 1$) indicates that the shear-thinning is insignificant in our experiment. The important decrease in viscosity η will appear for shear-rates $\dot{\gamma}$ higher than those relevant here.

For the non-Newtonian solution, an oscillatory test was also performed. A deformation of 3% was imposed, and the frequency of oscillation was varied from 0.01 to 100 s^{-1} during two periods for each point. With these measurements, the elastic G' (empty symbols) and viscous modulus G'' (filled symbols) are obtained. We observe a viscoelastic behavior, where the elastic property is dominant at low shear rate. This is in agreement with what has already been observed for such polymer solutions [22]. The relaxation time can be approximated as the time where the two modulus are equals. This is represented in Figure 1**d** as f_r, and we estimate the relaxation time $\tau_r = 1/f_r = 10$ s.

3. Experimental observations : Different regimes

The experiment is performed by injecting oil at the bottom of the fluid column, using a plastic syringe. The oil volume V is not measured a priori, instead it is estimated by image analysis, considering that for small drops, the volume corresponds to the one of a sphere of diameter D : $V = \pi D^3/6$ (Figure 3**a**), and for the bigger ones it is the sum of a cone of height H and a hemisphere of diameter D : $V = \pi D^2 H/12 + \pi D^3/12$ (Figure 3**b-e**). To insure good statistics, we reproduce the experiment 50 times and varying the volume V from 0.01 to 0.47 mL. Also by image analysis, we detect the position of the front of the drop to determine its velocity. Figure 2**a** presents the evolution of the vertical position z of the front of the drop as a function of time t for a drop of volume $V = 0.36$ mL. For all cases, we observe that the vertical position is linear in time t; the rising velocity U is then computed by a simple linear regression. Figure 2**b** shows the rising velocity U of the drop as a function of its volume V. The rising velocity increases slowly with the volume until it reaches a critical volume

Preprints (www.preprints.org) | NOT PEER-REVIEWED | Posted: 30 May 2018 doi:10.20944/preprints201805.0444.v1

Peer-reviewed version available at Fluids 2018, 3, 54; doi:10.3390/fluids3030054

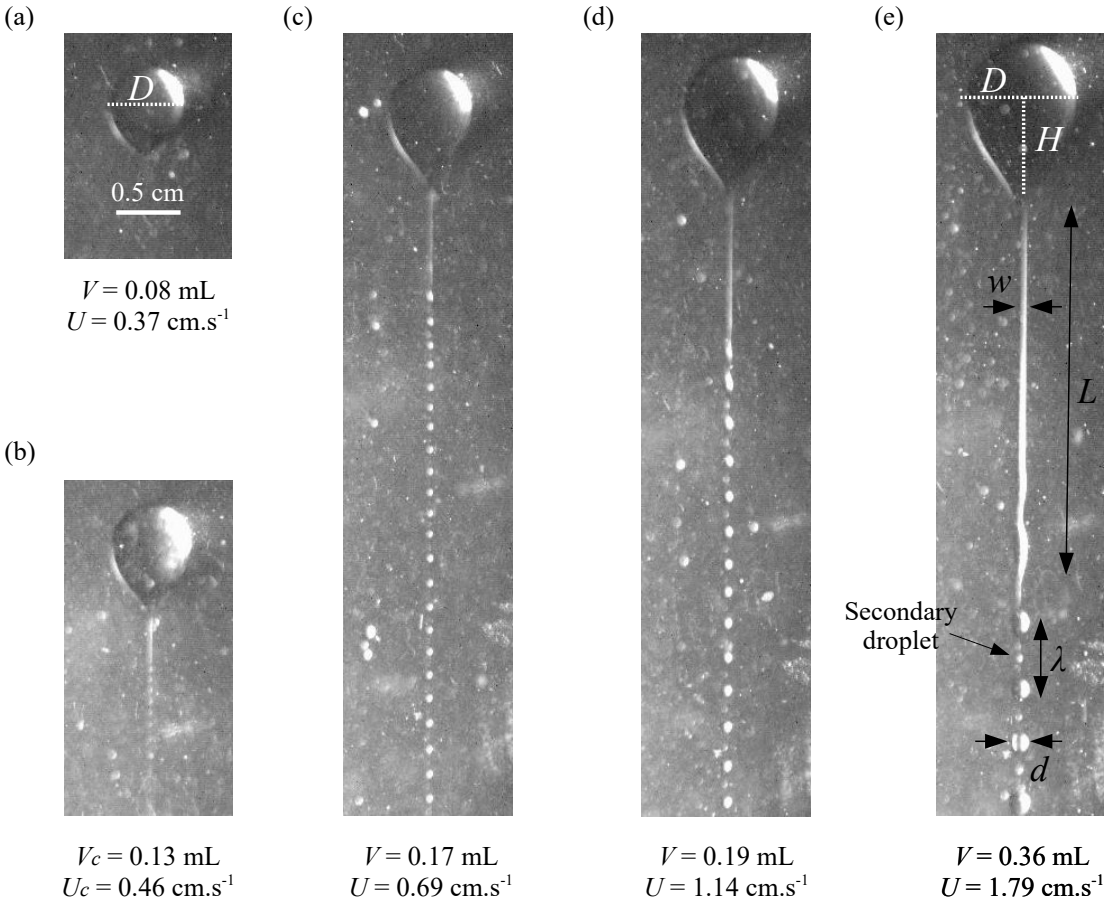

Figure 3. Different regimes observed : (**a**) Before the tail appears ; (**b**) At the critical volume V_c=0.13 mL where there is the tail appearance. We can see very small droplets appearing behind the tail of the main drop ; (**c-d-e**) Instability for different volumes. We can observe that the tail length L, the width of the tail w, the distance between two droplets λ and the droplets diameter d increases with the volume. Those are defined in (**e**) and this will be discuss in detail in section 4.

(V_c=0.13 mL). At this volume, a small velocity jump is observed and a tail appears at the rear of the drop. This velocity jump has already been reported in literature as the velocity discontinuity [14–18]. This appears for bubbles and drops rising in a viscoelastic surrounding fluid, and is directly linked with the appearance of a negative wake behind the bubble/drop. Above the critical volume V_c, the rising velocity U increases more rapidly with the volume V. Considering the non-Newtonian properties of the surrounding fluid (shear-thinning and viscoelastic), it is not possible to predict the shape of the curve over this critical volume, but many other experimental examples have reported similar behavior for drops or bubbles [14,19–21,23].

In terms of dimensionless numbers, it is common to use the Reynolds number Re and the Deborah number De. The Reynolds number compares the inertial forces of the flow with the viscous forces : $\mathrm{Re} = \rho UD/\eta = \rho UD/K\dot{\gamma}^{n-1}$, where ρ is the density of the surrounding fluid, U the velocity of the drop, D the diameter of the drop and η the viscosity. In our case, the fluid is shear thinning, so the viscosity changes with the shear rate. A common way to account this problem is to define the shear-rate as the ratio of velocity and diameter of the drop $\dot{\gamma} = U/D$, and to use this in the rheological measurements using the formula $\eta = K\dot{\gamma}^{n-1}$ where $n = 0.87$ and $K = 1.10$ (see section 2) We obtain finally a modified Reynolds number scaling as $\mathrm{Re} = U^{2-n}\rho D^n/K$ (see for instance [24]). This gives us a Reynolds number varying from 5×10^{-3} to 2.39. This small Reynolds number shows that inertial

effects are negligible. The Deborah number compares the viscoelastic relaxation time scale and the observation time scale : $\mathrm{De} = \tau_r/\tau_o$. We can define the observation time scale as the inverse of the shear rate : $\tau_o = 1/\dot{\gamma} = D/U$. For the relaxation time scale, we can estimate it as the time where there is the crossover between the elastic modulus G' and the viscous modulus G'' (see section 2). We measure this relaxation time as $\tau_r = 1/f_r = 10$ s. In our experiment, we have the Deborah number varying from 2.2 for the largest drops to 4.2 for the smallest ones. This value being larger than one, indicates that we will have important elastic effects appearing.

Figure 3 shows the different regimes of the drops as the volumes V increases. First, at small volumes (Figure 3**a**, the scale is reported on this image and is the same for all), the drop is spherical and no significant shape alterations are detected. When the drop reaches the the critical volume V_c (Figure 3**b**), a tail appears. According to Ortiz et al. [19] and Zenit & Feng [17], the appearance of the tail coincides with the formation of a negative wake. This tail will undergo a capillary instability where droplets are produced. At the critical volume, the tail is very small as are the droplets released. For the rest of the article we will use the term droplets for the liquid released behind the tail and drop for the main one. When the volume is increased (Figure 3**c-e**), we observe that the tail grows bigger in length L and width w, as well as the droplets diameter d and the distance between two droplets λ. Those values are defined in Figure 3**e** which correspond to the drop in Figure 2**a**. One important fact to note is that the volume the original drop V is not constant since it releases droplets. This will be more discussed in section 5. Note that secondary smaller droplets appear for the biggest drops ($V > 0.25$ mL, Figure 3**e**). The formation of such droplets has been discussed previously in [25]. In this article we will focus on the main droplets formation.

4. Droplet formation

4.1. Tail size

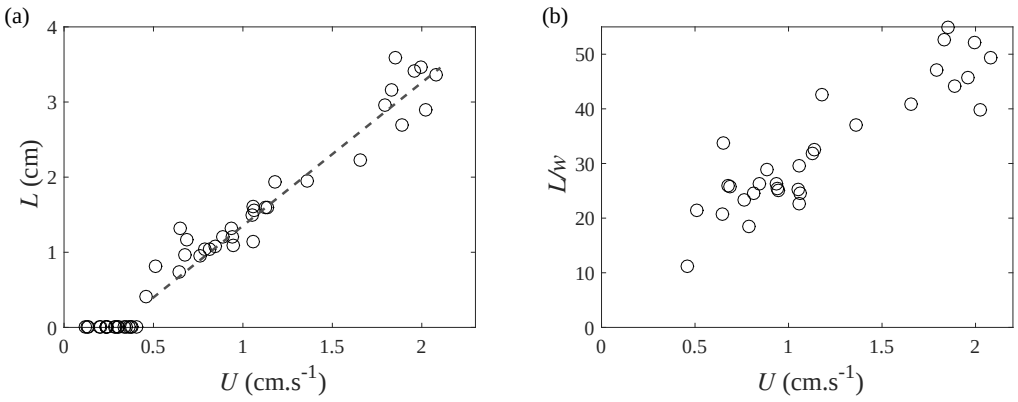

Figure 4. (**a**) Tail length L as a function of the velocity of the drop U. We see clearly a critical velocity U_c where the tails appears (corresponding to a critical volume V_c). The tail length grows linearly with the speed of the drop (dashed line). (**b**) Tail aspect ratio L/w as a function of the drop velocity V. The tail has a very elongated shape.

From the images the size of the tail behind the drop can be readily measured. We can obtain its width w and its length L, defined in Figure 4**e**.

Since we observe the drop in a terminal condition, we do not observe the initial formation of the tail. As for the volume of the drop, the length L and width w of the tail might change during the rising, since droplets are emitted, but once again, we did not observe a significant diminution of either the length or the width of the tail over the height of the camera window (12 cm). We measured the length L and the width w once the tail was fully visible in the images. Figure 4**a** shows the length of the tail as a function of the velocity of the drop U. We observe that under a critical velocity V_c, the tail does not

appear. The length of the tail and the drop velocity U are linearly related, from a length of 0.5 cm up to 3.6 cm, with a slope of 1.5 s (dashed line, Figure 4**a**). We will, discuss the value of this slope in the discussion section.

Figure 4**b** shows the tail aspect ratio L/w as a function of the drop velocity U. This aspect ratio is between 10 (for the drop at the transition), up to 50 for the largest drops. This shows that the tail is very long compare to its width, the width being for the smallest tail of about 0.035 cm to 0.075 cm for the biggest one. The fact that the curve increases, show that the tail will grow more rapidly with the velocity U in length L than in width w. This is physically intuitive, as the main driving force for the length of the tail is the strong non-Newtonian behaviour of the fluid, while the width of the tail is controlled by interfacial forces that are much smaller (as discussed in section 5).

4.2. Emission period and wavelength

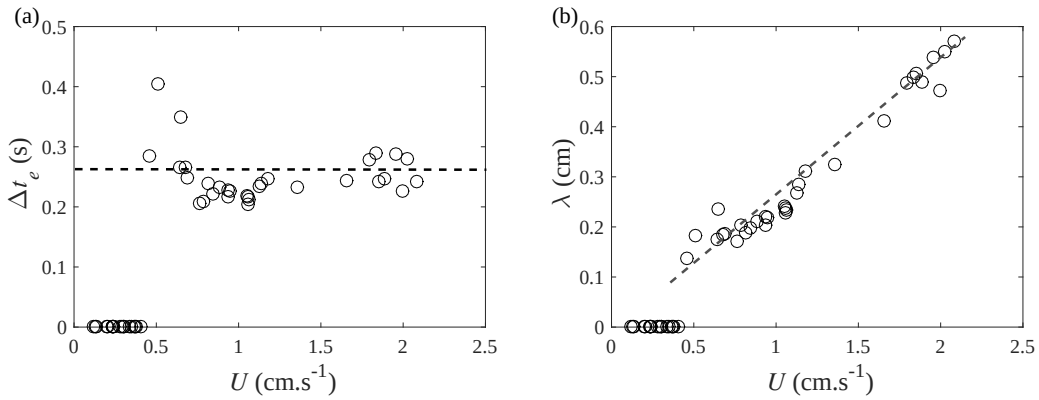

Figure 5. (**a**) Period of emission Δt_e of the droplets (average time between two droplets appearance), as a function of the drop velocity U. Except close to the critical volume, this period seems roughly constant (dashed line, $\Delta t_e = 0.27$ s), which corresponds at a frequency of emission f_e of 3.37 Hz. (**b**) Wavelength λ (average distance between two droplets), as a function of the drop velocity U. The dashed line represent the linear adjustment.

In Figure 3**b-e** we observe that the breakup of the tail is very regular in terms of spatial position (wavelength λ), and since the drop and the tail rises at a constant velocity, it is also regular in emission period Δt_e (for a given volume and velocity).

The Figure 5**a** shows the average time Δt_e (or emission period) between two droplets emitted, as a function of the velocity of the drop. Except at the critical velocity V_c, the period of emission of droplets Δt_e is roughly constant and has a value contained between 0.2 and 0.3 seconds. This results from a competition between the width w of the tail and the velocity U of the drop. For small velocity, the tail is thinner, so would tend to break more easily, and at higher velocity, the drainage of the tail is more rapid, which also helps the breakup. At the end, the time between two droplets emitted will be roughly the same for all velocity.

Figure 5**b** shows the average distance between two droplets λ, as a function of the velocity of the drops U. This distance increases importantly with velocity, which is in agreement with the constant emission period Δt_e : since the tail velocity increases with the volume (and the drop velocity), and the emission time between two drops is almost constant, this implies that the distance between two drops will increase with the velocity of the drop. We have a linear relation between λ and U for the drops over the critical volume V_c, with a slope of $\Delta t_e \approx 0.27$ s (dashed line, Figure 5**b**), which is in accordance with Figure 5**a**. We can compute the frequency of emission of the droplets, if we assume that the velocity is constant during one run, which gives us $f_e = 1/\Delta t_e \approx 3.37$ s^{-1}.

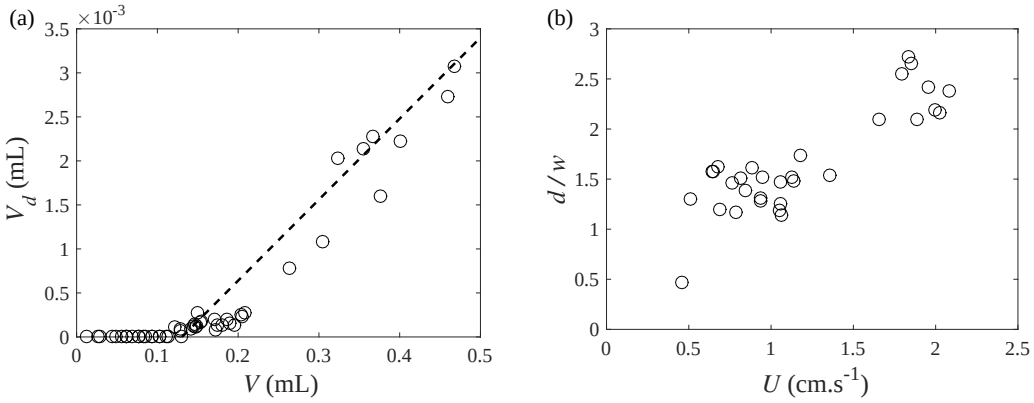

Figure 6. (**a**) Mean volume of the droplets V_d as a function of the volume of the drop V. We observe an important increase which is coherent with Figure 3. The dashed line represent the linear regression that will be used in section 5. (**b**) Droplet diameter d divided by the tail width w as a function of the drop velocity U. We observe that except for the critical case, the diameter of the droplets is always bigger than the tail width.

4.3. Droplet size

We also analyse the size of the droplets created behind the principal drop. Once again, we observe that the size of the droplets is constant over the course of one experiment (for one given drop volume V). The contrast being better for the droplets than the drop, the uncertainty on the diameter gets to about 1 pixel, but is still important in comparison with the droplet diameter. To reduce the error, we measure the diameter for 10 different droplets, which decrease significantly the error, down to an estimated 5 percent. We used the same method to estimate the width of the tail, measuring the width at different heights and then averaging. Note also that we only consider the large droplets; the secondary smaller droplets were not measured. The Figure 6**a** shows the average volume of the droplets V_d as a function of the volume of the main drop V. The volume of the droplets V_d has been computed assuming that the droplet is a sphere : $V_d = 4/3\pi(d/2)^3$, where d is the diameter of the droplets (see Figure 3**e**). We observe that the volume of the droplets increase linearly with the volume of the drop, the bigger the drop, the bigger are the droplets. The dashed line represent a linear regression, that will be discussed in the discussion.

The Figure 6**b** shows the normalized droplet diameter d/w as a function of the velocity of the drop U. We observe that this ratio increases with the velocity, and most of all, its value is always larger than one (except for one point at the transition), which means that the droplets are larger then the tail before it breaks. This can be explained by a simple mass conservation argument. The volume of oil before the break corresponds to the volume of a column of width w and height λ (for one wavelength), and also to the volume of one droplet of diameter d. We can write this volume as $V_d = \pi/4\lambda w^2 = 1/6\pi d^3$. Therefore,

$$\frac{d^2}{w^2} = 3/2\frac{\lambda}{d} \tag{1}$$

Considering that the distance of between two droplets is much bigger than the size of the droplet except at the critical volume (see Figure 3), we have $\lambda/d > 1$, and so the diameter of the droplet d will be bigger than the width of the tail w.

5. Discussion

5.1. Tail apparition

We observe that a tail appears behind the drop for a volume larger than the critical one $V_c = 0.13$ mL. This critical volume correspond to a discontinuity in velocity (Figure 2**b**), and discontinuity also corresponds to the appearance of a negative wake behind the drop. This discontinuity and negative have been already studied in various cases, for bubbles [14–16,18–21], and for drops [11,17,19]. In some of these works particle image velocimetry technique is used to show the existence of this negative wake. The negative wake results directly from the viscoelastic behaviour of the surrounding fluid. The bubble displacing the fluid vertically will create a counter flow behind it. This phenomena only appears if the rising velocity is large enough. For smaller bubbles/drops,considering that the fluid is viscous, the flow is in a laminar regime, and the bubble will have a round shape, controlled by the capillary forces.

The main difference between the drop case and the bubble case is that the interfacial tension between the air and the fluid is larger than in the case of two liquids. The bubble shape will then remain the same over the course of the experiment (except in the case of other instabilities appearing [23]), while in the case of a drop, this interface is more deformable, and the tail will be able to grow due to the negative wake [19]. Since the velocity increases with the volume (Figure 2**b**), the negative wake will also be more important and the tail length L will rise (Figure 4**a**). Its width w will also grow with the volume V, but slower than its length (Figure 4**b**). This is due to the fact that the drag effect (or negative wake) is confined laterally in a small zone behind the drop, so the horizontal extension will not be large (see PIV in [19]).

5.2. Tail breakup

In our experiment, the drop is made of oil which is Newtonian. For the case where the drop is non-Newtonian, the tail can grow more, due to its elongational viscosity [19]. The breakup is then observed at a much bigger distance from the bubble. In the Newtonian case, the non-Newtonian surrounding fluid will create an elastic pressure on the tail, and will then break it into smaller droplets. This droplet emission will occur at the end of the tail at a distance going from 0.5 to 3.6 cm. This distance (which corresponds to what we called the tail length L) will vary linearly with the velocity U, with a slope of 1.5 s (dashed line, Figure 4**a**).

This type of thread breakup is similar to the Rayleigh-Plateau instability [25,26]. In the case of a thin thread of liquid flowing in an other fluid (gas or liquid), a natural destabilisation occurs and the thread destabilizes in droplets. This rupture comes from capillary effects. The temporal evolution of this rupture is hard to predict, as it has to take into account the velocity of the fluid inside the thread (the tail in our case). We do not have access to this velocity, and is hard to predict since it results from a the negative wake. We observe that the time between two consecutive droplets emission Δt_e does not depend on the velocity of the drop U (Figure 5**a**), and since the drops rises at constant velocity, there the distance between two droplets emitted λ will increase linearly with the velocity U. Given that the wavelength λ is bigger than the tail width w, the diameter of the droplets d will be larger than the tail width w, except for the bubble at the critical volume (Figure 6**b** and Equation 1).

A typical way to describe such type of instabilities is to look at the capillary number and capillary length. The capillary number describes the ratio between the capillary forces and the viscous forces : $\mathrm{Ca} = \eta U/\sigma$, where σ is the interfacial tension between the two fluids. In our case, we have a proportionality between the wavelength of emission λ, and the velocity U. The viscosity will not change significantly at the tail surrounding : the velocity field is damped by viscosity effects, and the shear-thinning power law for the fluid is small ($n = 0.87$, Section 2) in the shear-rates considered. We then have a direct proportionality between the capillary number Ca and the wavelength λ :

$$\lambda = \Delta t_e U = k.\mathrm{Ca} \tag{2}$$

where k is a constant coefficient with the dimension of a length, which implies that $k = \Delta t_e \sigma/\eta$. An important dificulty is to evaluate the interfacial tension σ. This is not a trivial problem and we do not have the means to measure this interfacial tension. However, we can assume that it is of the order of magnitude of the interfacial tension between water and oil, which has been measured in [27] and its value is $\sigma \approx 35$ mN/m. By taking $\eta \approx 0.9$ Pa.s, we obtain that $k \approx 1.05$ cm. The capillary length can be defined as $l_c = \sqrt{\sigma/\Delta\rho g}$, where $\Delta\rho$ is the density difference between the two fluids, and g is the gravitational acceleration. When computed, we obtain $l_c \approx 1.29$ cm. We observe that this is the same order of magnitude than k for our experiment. Therefore $k \approx l_c$, which indicates that, indeed, the breakup of the tail results from capillary instability. Clearly, l_c and k are not identical, k being 30 % smaller than l_c. The calculation of l_c does not take into account the viscoelastic properties of the surrounding fluid, and also that the interfacial tension is not measured directly. Nevertheless, these scaling arguments indicate that indeed the tail is fragmenting mainly as a result of capillary instability and the viscoelastic effects are secondary. Although there have been some studies that have addressed the effects of viscoelasticity in the fragmentation process of a filament [28,29] the present case (the instability of Newtonian filament immersed in a viscoelastic liquid) has not been yet addressed.

5.3. Volume Loss

It is important to evaluate the role of volume change for the main drop, resulting from the droplets emitted at the tail. In all cases, we assumed that the drop volume V was constant. This assumption is supported by two facts. First, in Figure 2**a**, the bubble rises at a constant velocity, which would not have been the case if the volume had varied significantly. Secondly, Figure 6**a** show that the volume of the droplets V_d, is remains smaller than 0.65 percent of the main drop volume, for the largest drops. In this case, only 20 droplets are emitted over the experiment, which makes (in the worst case scenario) a volume loss around 13 percent of the initial drop volume.

However, the question of the volume change can have an important impact, especially considering possible applications. A simple model is proposed, to predict the volume of the droplets in an infinitely long liquid column. First, by using the linear regression in Figure 6**a**, we can predict the volume of a droplet knowing the volume of the main drop. Then, assuming that the emission frequency of droplets is constant $f_e = 3.37\ \mathrm{s}^{-1}$ (Figure 5**a**), we can write the following differential equation for the volume change :

$$\frac{\mathrm{d}V}{\mathrm{d}t} = -f_e V_d = -f_e(\alpha.V + \beta) \tag{3}$$

where $\alpha = 9.2 \times 10^{-3}$ and $\beta = -1.2 \times 10^{-3}$ mL are the slope and intercept of the dashed line in Figure 6**a**. Integrating, we obtain

$$V(t) = V_0 \exp(-f_e.\alpha.t) + \frac{\beta}{\alpha}(\exp(-f_e.\alpha.t) - 1) \tag{4}$$

where V_0 is the initial drop volume (taken to be 0.5 mL). This expression, if used carelessly, will predict a negative volume value for long times; however, one must consider that the droplets will no longer be emitted once the volume $V(t)$ reaches the critical volume (V_c =0.13 mL). The drop will then rise with a constant volume V_c and a constant velocity $U_c \approx 0.46$ cm.s^{-1}. Figure 7**a** shows the volume evolution $V(t)$ as a function of time t. The critical volume V_c is reached at a time $t_c = 28.5$ s.

We can use a linear regression between the volume and the velocity over the critical volume in Figure 2**b** which gives $U(t) = 7.6V(t) - 0.52$. Figure 7**b** shows the velocity of the drop U, as a function of time t, the velocity decreases from 3.3 cm.s^{-1} to U_c =0.46 cm.s^{-1}. This is clearly only a first order approximation, since the relation between the volume and velocity is most likely non linear. It allows

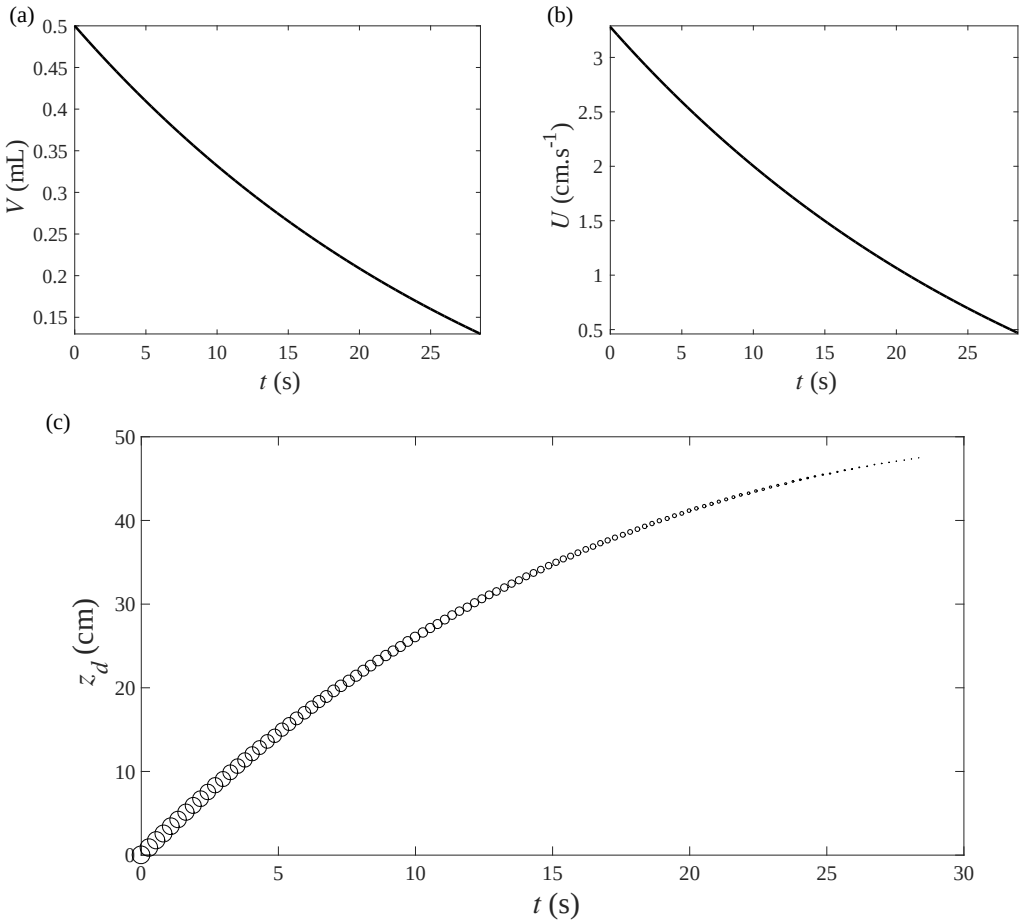

Figure 7. (**a**) Volume V evolution as a function of time t. The critical volume $V_c = 0.13$ mL is reached after a time $t_c = 28.5$ s. (**b**) Velocity of the droplet U as a function of time t. (**c**) Velocity of the droplet U as a function of time t. (**c**) Position of the droplets z_d as a function of time t. The size of the markers represents the volume of each droplet.

us to continue the integration. We can then compute the position $z(t)$ of the drop as a function of time as :

$$z(t) = \int_0^t U \mathrm{d}t' = \int_0^t (7.6V(t) - 0.52)\mathrm{d}t' \tag{5}$$

For simplicity, we will not write down this integral (it implies exponential integrals). Figure 7**c** shows the position of the droplets emitted z_d, as a function of time t. The droplets are emitted every $\Delta t_e = 0.27$ s, and the marker size is proportional to the volume of the droplets. The drop will reach its critical volume at a position $z_c = 47.6$ cm, and then will rise at its constant velocity, without emitting new droplets. The volume of the droplets emitted will vary from $V_d = 0.0034$ mL at the beginning, and will tend to 0 when we approach the critical volume.

This simple model gives us an order of magnitude of what should be expected in terms of time t_c and height z_c for the bubble to reach its critical volume V_c. This is in agreement with what was shown before : t_c is much bigger than the time of our experiment (10 s), and z_c also much bigger than the 12 cm where we observed the rise, so the model holds some consistency. This could be used to predict droplets encapsulation in other cases, considering a tall enough column.

6. Conclusion and perspectives

In this article, we investigated the instability occurring at the tail of an oil drop rising in a viscoelastic fluid. We observe that this leads to the formation of small droplets, that can be controlled in

size. It is interesting to note that the practical implications of such behaviour (cusp and tail formation with fragmentation) had not been discussed previously. In this article, we use the results of a particular case (two specific fluids), but the understanding of the process can be generalized for other fluid systems. We plan to further pursue this idea in the future.

Author Contributions: Investigation, Raphael Poryles; Writing—Original Draft Preparation, Raphael Poryles; Supervision, Roberto Zenit

Funding: Raphael Poryles acknowledges the support of DGAPA-UNAM for postdoctoral support.

Acknowledgments: The rheological measurement have been performed using a rheometer owned by Elsa De la Calleja from IIM-UNAM.

Conflicts of Interest: "The authors declare no conflict of interest."

References

1. Wu L, Chen P, Dong Y, Feng X and Liu B F. Encapsulation of single cells on a microfluidic device integrating droplet generation with fluorescence-activated droplet sorting. *Biomed Microdevices* **2013**, *15*, 553-560.
2. Teh S Y, Lin R, Hung L H and Lee A P. Droplet microfluidics. *Lab Chip* **2008**, *8*, 198-220.
3. Theberge A B, Courtois F, Schaerli Y, Fischlechner M, Abell C, Hollfelder F and Huck Wilhelm T S. Microdroplets in Microfluidics : An Evolving Platform for Discoveries in Chemistry and Biology. *Angewandte Chemie International Edition* **2013**, *49*, 5846-5868.
4. Mark D, Haeberle S, Roth G, Von Stetten F and Zengerle R L. Microfluidic Lab-on-a-Chip Platforms: Requirements, Characteristics and Applications. In *Microfluidics Based Microsystems*; Kakaç S, Kosoy B, Li D and Pramuanjaroenkij A. Eds.; Springer Netherlands, 2010; pp. 305-376, 978-90-481-9029-4.
5. Garstecki P, Fuerstman M J, Stone H A, and Whitesides G M. Formation of droplets and bubbles in a microfluidic T-junction—scaling and mechanism of break-up. *Lab Chip* **2006**, *6*, 437-446.
6. De Menech M, Garstecki P, Jousse F and Stone H. Transition from squeezing to dripping in a microfluidic T-shaped junction. *J Fluid Mech* **2008**, *595*, 141-161.
7. Arigo M T and McKinley G H. An experimental investigation of negative wakes behind spheres settling in a shear-thinning viscoelastic fluid. *Rheol Acta* **1998**, *37*, 307–327.
8. Bisgaard C and Hassager O. An experimental investigation of velocity fields around spheres and bubbles moving in non-Newtonian liquids. *Rheol Acta* **1982**, *21*, 537-539.
9. Broadbent J and Mena B. Slow flow of an elastico-viscous fluid past cylinders and spheres. *Chem Eng J* **1974**, *8*, 11-19.
10. Caswell B, Manero O and Mena B. Recent developments on the slow viscoelastic flow past spheres and bubbles. In: DM Binding and K Walters (eds.) *Rheology reviews* **2004**, 197-223.
11. Chhabra RP. Bubbles, Drops and Particles in Non-Newtonian Fluids. CRC Press *Technology & Engineering* **1993**.
12. Manero O and Mena B. On the slow flow of viscoelastic fluids past a circular cylinder. *J Non-Newtonian Fluid Mech* **1981**, *9*, 379-387.
13. Mena B, Manero O and Leal LG. The influence of rheological properties on the slow flow past spheres. *J Non-Newtonian Fluid Mech* **1987**, *26*, 247-275.
14. Herrera-Velarde JR, Zenit R, ChehataD and Mena B. The flow of non- Newtonian fluids around bubbles and its connection to the jump discontinuity. *J Non-Newtonian Fluid Mech* **2003**, *111*, 199-209.
15. Rodrigue D and De Kee D. Bubble velocity jump discontinuity in polyacrylamide solutions; a photographic study. *Rheol Acta* **1998**, *37*, 307-327.
16. Rodrigue D, De Kee D and Chan Man Fong C. Bubble velocities: further developments on the jump discontinuity. *J Non-Newtonian Fluid Mech* **1998**, *79*, 45-55.
17. Zenit R and Feng J J. Hydrodynamic Interactions Among Bubbles, Drops, and Particles in Non-Newtonian Liquids. *Annu Rev Fluid Mech* **2018**, *50*, 505-534.
18. Astarita G and Apuzzo G. Motion of gas bubbles in non-Newtonian liquids. *AICHE J* **1965**, *11*, 815-820.
19. Ortiz S L, Lee J S, Figueroa-Espinoza B and Mena B. An experimental note on the deformation and breakup of viscoelastic droplets rising in non-Newtonian fluids. *Rheol Acta* **2016**, *55*, 879-887.
20. Hassager O. Negative wake behind bubbles in non-Newtonian liquids. *Nature* **1979**, *279*, 402-403.

21. Soto E, Goujon C, Zenit R and Manero O. A study of velocity discontinuity for single air bubbles rising in an associative polymer. *Phys Fluids* **2006**, *18*, 121510.
22. Ghannam MT and Esmail MN. Rheological properties of aqueous polyacrylamide solutions. *J Appl Polym Sci* **1998**, *69*, 1587–1597.
23. Poryles R and Vidal V. Rising bubble instabilities and fragmentation in a confined polymer solution. *J Non-Newton Fluid Mech* **2017**, *241*, 26-33.
24. Palacios-Morales C and Zenit R. The formation of vortex rings in shear-thinning liquids. *J Non-Newton Fluid Mech* **2013**, *194*, 1-13.
25. Lister J R and Stone H A. Capillary breakup of a viscous thread surrounded by another viscous fluid. *Phys of Fluid* **1998**, *10*, 2758-2764.
26. De Gennes PG, Brochard-Wyart F and Quéré D. Capillary and Wetting Phenomena — Drops, Bubbles, Pearls, Waves. Alex Reisinger (trans.) *Springer* **2002**.
27. Peters F and Arabali D. Interfacial tension between oil and water measured with a modified contour method. *Coll Surf A* **2013**, *426*, 1-5.
28. Clasen C, Eggers J, Fontelos M A, Li J and McKinley G. The beads-on-string structure of viscoelastic threads. *J Fluid Mech* **2006**, *556*, 283-308
29. Deblais A, Velikov K P and Bonn D. Pearling instabilities of a viscoelastic thread. *Phys Rev Lett* **2018**, *120*, 194501.